

# Finite temperature correlation functions

D.S.Kuzmenko<sup>1</sup>, Yu.A.Simonov<sup>2</sup>

*Institute of Theoretical and Experimental Physics,  
117218, Moscow, Russia*

## Abstract

Lattice measurements of the Pisa group (A.Di Giacomo et al., hep-lat/9603018) are analyzed numerically and parameters of correlation functions are extracted from the data – both below and above deconfinement temperature  $T_c$ . Gluon condensate is found for six temperatures in the interval  $0.956 T_c - 1.131 T_c$  and field distributions in deconfined phase are obtained.

## 1 Introduction

Study of field distributions around static quarks has a long history. The information obtained both analytically and on the lattice, has an important meaning in several respects. Firstly, it demonstrates clearly the appearance of the QCD string between the charges in the confining phase and the detailed contents of this fields in this string; e.g. the string consists of color-electric fields to more than 90%. Secondly, since the string enters in many dynamical quantities, such as static interquark potential, spin-dependent forces for heavy quarkonia etc., one can easily compute the latter from the string field distributions.

Finally, and this is the purpose of the present paper, the phenomenon of deconfinement is not fully understood from the point of view of the string and field distributions.

What actually happens when temperature  $T$  exceeds the critical value – the string disappears or distribution of fields is drastically changed, so that to compensate the string tension?

Happily there exist numerical lattice measurements of field correlators near the critical temperature  $T_c$ , made by the Pisa group [1], where both electric and magnetic correlators are found with good accuracy. These data clearly demonstrate the strong suppression of color-electric component above  $T_c$  and persistence of color-magnetic components.

The purpose of the present paper is twofold. First, we reanalyze the data of [1] in terms of correlators  $D^{E,B}$  and  $D_1^{E,B}$  which are better understood from the point of view of perturbative and nonperturbative contributions [2]. There was e.g. shown that the string tension  $\sigma$  ("conventional" electric or "spatial" magnetic) is expressed directly through the  $D^{E,B}$  but not the  $D_1^{E,B}$ . Given the simple assumption of behavior  $D^{E,B}(x)$  and  $D_1^{E,B}(x)$  in all region of  $x$ , we obtain the behavior of gluon condensate near the  $T_c$  (which is defined by  $D^{E,B}(0)$  and  $D_1^{E,B}(0)$ ).

Secondly, using the obtained  $D^{E,B}(x)$  and  $D_1^{E,B}(x)$ , we calculate the color field distributions around static quarks in the deconfined phase. We perform these calculations using the connected probe [3] in the framework of Field Correlator Method (FCM) [4,5]. We study in detail two possible from the deconfinement point of view regimes, corresponding to two forms of  $D(x)$ , extracted from lattice data [1]. In the first one the string disappears and

---

<sup>1</sup>e-mail: kuzmenko@heron.itep.ru

<sup>2</sup>e-mail: simonov@heron.itep.ru

in the second (less appealing physically, but more supported by the lattice data) the string becomes a coaxial cable with the empty core.

The paper is organized as follows.

In section 2 a short description is given of our fitting procedure of magnetic correlators at any  $T$  and the electric correlators at  $T < T_c$ , while in section 3 more prolonged one is given for electric correlators at  $T > T_c$ . The section 4 is devoted to the behaviour of the gluonic condensate below and above  $T_c$ . In section 5 the detailed equations for field distributions around static quark and antiquark are given and illustrated graphically.

In the concluding section results of the paper are summarized and most likely physical picture of fields in the deconfinement phase is given.

## 2 Fitting data with nonzero string tension

In this section we consider magnetic correlators in all temperature region and electric correlators at  $T < T_c$  since both of them produce (e.g. spatial) nonzero string tension. We fit the data [1] using the method of least squares [6]. To begin with, we express the functions  $D_{||}(x)$ ,  $D_{\perp}(x)$  through the  $D(x)$ ,  $D_1(x)$  and represent the lasts as sums of nonperturbative (NP) and perturbative (P) (diverging at zero) contributions. This is the procedure used by A.Di Giacomo et al.[7] when analyzing the correlation functions at zero temperature. The difference is that we should distinguish electric and magnetic correlators due to the finite temperature theory has only the  $O(3) \times O(1)$  symmetry.

We fit distributions of

$$D_{||}^{E,B}(x) = D^{E,B}(x) + D_1^{E,B}(x) + \frac{x}{2} \frac{\partial D_1^{E,B}(x)}{\partial x} \quad (1)$$

and

$$D_{\perp}^{E,B}(x) = D^{E,B}(x) + D_1^{E,B}(x) \quad (2)$$

electric and magnetic correlation functions in the range from 0.4 to 1 fm. All points are measured at  $x_4 = 0$ . In this section we parametrize functions as follows:

$$D(x) = A \exp(-x/\lambda_A) + \frac{a}{x^4} \exp(-x/\lambda_a), \quad (3)$$

$$D_1(x) = B \exp(-x/\lambda_B) + \frac{b}{x^4} \exp(-x/\lambda_b). \quad (4)$$

Fitting the magnetic functions (which are close to exponentials), we set in (3),(4)  $\lambda_a = \lambda_b = \lambda_B$ , thus using  $k = 6$  fitting parameters. Given  $N = 12$  number of data, we have as a result  $n = N - k = 6$  number of degrees of freedom. The results are shown in Tables 1. One-standard-deviation errors  $\Delta\alpha_i$  are determined from the equation  $\chi^2(\alpha_1, \dots, \alpha_i + \Delta\alpha_i, \dots, \alpha_k) = \chi^2(\alpha_1, \dots, \alpha_k) + \Delta\chi_k^2$ , where  $\alpha_i$  are fitted parameters and  $\Delta\chi_1^2 = 1$ ,  $\Delta\chi_4^2 = 4.75$ ,  $\Delta\chi_6^2 = 7$  [6].

Preliminary fitting of electric data at  $T = 0.956T_c$  with parameters of (3),(4) gave unacceptable big  $\chi^2$  due to the end points of  $D_{||}^E$  and  $D_{\perp}^E$ ;  $\lambda_A$ ,  $\lambda_a$  and  $\lambda_b$  were found close to each other. Therefore we have remove mentioned points and set  $\lambda_A = \lambda_a = \lambda_b$  to get the reasonable fit (Table 2).

Preliminary fitting of electric data at  $T = 0.978T_c$  have shown that  $\chi^2$  is also too big and besides that  $\lambda_A$  is close to  $\lambda_b$  and  $\lambda_B$  to  $\lambda_a$ . Therefore we set  $\lambda_b = \lambda_A$  and  $\lambda_a = \lambda_B$ . To improve  $\chi^2$ , we enlarge two times the error of the last point of  $D_{||}$  (Figure 1). This procedure

however leads to sizable deviation e.g. of parameter  $A$  (Table 2). (One can make sure from Figure 1 that this point is largely off the exponential curve, which may be connected to the lattice size effects.)

### 3 Fitting electric data in the deconfinement region

$D_{||}^E$  above  $T_c$  have a drop that is presumably related with the deconfinement transition, when the string tension of area law asymptotics of Wilson loop for static quarks disappears,

$$\sigma = \frac{1}{2} \int dx_1 dx_4 D^{E,NP}(x_1, x_4) = 0. \quad (5)$$

In this region we should alter the form of  $D$  (3) to justify (5). It is naturally to set

$$D^{NP}(x) \equiv 0. \quad (6)$$

(We omit subscript "E" here and in what follows in this section.) As we shall see below, this form assures reasonably well fit of data. Let us propose another form of  $D$  to ensure good fitting of data. We suppose now more constrained  $O(4)$  symmetry:  $D(\mathbf{x}^2, x_4^2) = D(\mathbf{x}^2 + x_4^2) \equiv D(x^2)$  to get

$$\sigma = \frac{\pi}{2} \int_0^\infty dx^2 D^{NP}(x^2) = \frac{\pi}{2} \int_0^\infty dx^2 D_{||}^{NP}(x^2) = 0. \quad (7)$$

To better reproduce the mentioned drop of data, we set  $D_{||}^{NP}(x) \equiv 0$ , i.e.

$$D^{NP}(x) = -D_1^{NP}(x) - \frac{x}{2} \frac{\partial D_1^{NP}(x)}{\partial x}, \quad (8)$$

leaving meanwhile  $D_1$  in form (4) intact.

So far we have adopted two forms of  $D(x)$ :

$$D(x) = \frac{a}{x^4} \exp(-x/\lambda_a); \quad (9)$$

$$D(x) = B\left(\frac{x}{2\lambda_B} - 1\right) \exp(-x/\lambda_B) - \frac{a}{x^4} \exp(-x/\lambda_a). \quad (10)$$

We fit data on  $D_{||}$  and  $D_{\perp}$  at  $T = 1.011T_c$  in two ways, using (a): functions (9),(4) and (b): (10),(4). Having in mind the small number of data we set  $\lambda_a = \lambda_b = \lambda_B$  to have  $k = 4$ . Given  $N = 9$ , we obtain  $n = 5$  (Table 3). We see from the Table 3 the somewhat reasonable  $\chi^2/n = 1.7$  in case (a) and excellent  $\chi^2/n = 1.05$  in case (b).

At higher temperatures there are only two measurements of  $D_{||}$ , with values significantly less even than the errors of corresponding points of  $D_{\perp}$ . This circumstance allows us to subdivide the fitting procedure in two stages. At the first stage we fit the difference  $(D_{\perp} - D_{||})$  (cf. (1),(2)) by  $-x^2 \partial D_1 / \partial x^2$  (cf. (4)), and extract parameters  $(B, \lambda_B, b, \lambda_b)$ . At the second stage we fit (eventually, secondly)  $D_{\perp}$ , reproducing it (in two ways, due to two cases of  $D$ ) by the sum of  $D$  and  $D_1$  extracted from the first fit in forms (9) and (10) with  $\lambda_a = \lambda_b$  in both cases, and only the parameter  $a$  is allowed to vary (Table 4, Figure 2). One-standard-deviation errors are determined as described above, with  $k = 4$  at the first stage and  $k = 1$  at the second stage of fitting.

To summarize, at the first stage we fit the data by

$$D_{\perp}(x) = \frac{Bx}{2\lambda_B} \exp(-x/\lambda_B) + \frac{2b}{x^4} \left(1 + \frac{x}{4\lambda_b}\right) \exp(-x/\lambda_b) \quad (11)$$

and at the second stage in case (a) by

$$D_{\perp}(x) = B \exp(-x/\lambda_B) + \frac{a+b}{x^4} \exp(-x/\lambda_b) \quad (12)$$

and in case (b) by

$$D_{\perp}(x) = \frac{Bx}{2\lambda_B} \exp(-x/\lambda_B) + \frac{a+b}{x^4} \exp(-x/\lambda_b), \quad (13)$$

with all parameters of (12),(13) except  $a$  fixed by the first stage. One could see that (13) well reproduces (11) independently on  $B$  and  $\lambda_B$  at  $x \ll 4\lambda_b$ , i.e. in all measured region  $0.4\text{fm} < x < 1\text{fm}$  (see Table 4).

## 4 Temperature dependence of the gluon condensate

The gluon condensate is defined as

$$G_2 \equiv \frac{\alpha_s}{\pi} \langle F_{\mu\nu}^a F_{\mu\nu}^a \rangle. \quad (14)$$

At zero temperature the FCM reads

$$\begin{aligned} \frac{g^2}{N_c} \langle F_{\rho\sigma}^a(x') (T^a)_{\beta}^{\alpha} \Phi_{\gamma}^{\beta}(x', x) F_{\mu\nu}^b(x) (T^b)_{\delta}^{\gamma} \Phi_{\alpha}^{\delta}(x, x') \rangle &= (\delta_{\rho\mu} \delta_{\sigma\nu} - \delta_{\rho\nu} \delta_{\sigma\mu}) (D(h^2) + D_1(h^2)) + \\ &+ (h_{\mu} h_{\rho} \delta_{\nu\sigma} - h_{\mu} h_{\sigma} \delta_{\nu\rho} - h_{\rho} h_{\nu} \delta_{\mu\sigma} + h_{\nu} h_{\sigma} \delta_{\mu\rho}) \frac{\partial D_1(h^2)}{\partial h^2}, \end{aligned} \quad (15)$$

where  $h \equiv x - x'$ ,  $\alpha, \dots, \delta$  are color indices. At  $x = x' = 0$  one uses in (14)  $\text{tr} T^a T^b = \frac{1}{2} \delta^{ab}$  and get

$$\frac{g^2}{N_c} \langle F_{\mu\nu}^a F_{\mu\nu}^a \rangle = 12(D(0) + D_1(0)) \quad (16)$$

In what follows we shall use the zero temperature lattice results [7]:

$$D^{\text{NP}}(0) = 3.3 \cdot 10^8 \Lambda_L^4 = 129 \text{fm}^{-4}, \quad D_1^{\text{NP}}(0) = 0.7 \cdot 10^8 \Lambda_L^4 = 27 \text{fm}^{-4}. \quad (17)$$

From (15) one derives

$$\frac{g^2}{N_c} \langle E_i^a(0) E_i^a(0) \rangle = 3(D^E(0) + D_1^E(0)), \quad (18)$$

$$\frac{g^2}{N_c} \langle B_i^a(0) B_i^a(0) \rangle = 3(D^B(0) + D_1^B(0)), \quad (19)$$

where  $E_i = F_{0i}$  and  $B_i = \frac{1}{2} \epsilon_{klm} F_{lm}$ . Note that at finite temperature  $D^E$  and  $D^B$  acquire subscripts for symmetry breaking reason  $O(4) \longrightarrow O(3) \times O(1)$ . We have to distinguish electric and magnetic contributions from condensate:

$$\langle F_{\mu\nu}^a F_{\mu\nu}^a \rangle = \langle F^2 \rangle_{el} + \langle F^2 \rangle_{magn}, \quad (20)$$

where

$$\langle F^2 \rangle_{el} = \langle F_{0i}^a F_{0i}^a \rangle + \langle F_{i0}^a F_{i0}^a \rangle = 2\langle E_i^a E_i^a \rangle, \quad (21)$$

$$\langle F^2 \rangle_{magn} = \frac{1}{4}\epsilon_{ijk}\epsilon_{ijk}\langle F_{jk}F_{jk} \rangle + \frac{1}{4}\epsilon_{ijk}\epsilon_{ijk}\langle F_{kj}F_{kj} \rangle = 2\langle B_i^a B_i^a \rangle \quad (22)$$

Substituting (16), (18)–(22) into (14), one obtains that normalized gluonic condensate is

$$\frac{G_2(T)}{G_2} = \frac{D^E(0) + D_1^E(0) + D^B(0) + D_1^B(0)}{2(D(0) + D_1(0))}, \quad (23)$$

where all  $D$  mean its NP parts, i.e. corresponding parameters  $A$  and  $B$ . Table 5 shows the behavior of electric and magnetic condensates separately as well as  $G_2(T)/G_2$  as a whole.

Data on the normalized gluonic condensate (23) from Table 5 are plotted in Figure 3.

## 5 Field distributions around of deconfined quarks

In this section we consider the NP part of gluodynamical field generated by static  $Q\bar{Q}$  sources, measured by the connected probe [3]. The only nonzero components in this system is longitudinal (along quark axis) and transverse electric fields  $E_1(x_1, x_2)$  and  $E_2(x_1, x_2)$ , where  $x_1$  is coordinate along quark axis and  $x_2$  distance to the axis.

In case (a), when  $D^{\text{NP}} \equiv 0$ , NP part of  $D_1$  is  $D_1 = B \exp(-x/\lambda)$ , where  $x = \sqrt{x_1^2 + x_2^2 + x_3^2}$  (due to axial symmetry we may set  $x_3 \equiv 0$ ),  $\lambda$  means  $\lambda_B$ . In what follows we refer to the equations of [8]:

$$\langle E_1(x_1, x_2) \rangle_{Q\bar{Q}}^{(a)} = \int_0^R dx'_1 \int_{-\infty}^{\infty} dx'_4 \left( D_1(h^2) + (h_1^2 + h_4^2) \frac{\partial D_1(h^2)}{\partial h^2} \right) =$$

$$B(x_1 \sqrt{x_1^2 + x_2^2} K_1(\sqrt{x_1^2 + x_2^2}/\lambda) - (x_1 - R) \sqrt{(x_1 - R)^2 + x_2^2} K_1(\sqrt{(x_1 - R)^2 + x_2^2}/\lambda)), \quad (24)$$

$$\langle E_2(x_1, x_2) \rangle_{Q\bar{Q}} = \int_0^R dx'_1 \int_{-\infty}^{\infty} dx'_4 h_1 h_2 \frac{\partial D_1(h^2)}{\partial h^2} =$$

$$B x_2 (\sqrt{x_1^2 + x_2^2} K_1(\sqrt{x_1^2 + x_2^2}/\lambda) - \sqrt{(x_1 - R)^2 + x_2^2} K_1(\sqrt{(x_1 - R)^2 + x_2^2}/\lambda)), \quad (25)$$

where  $K_1$  is McDonald function. The total field is

$$\langle \mathbf{E} \rangle^2 = \langle E_1 \rangle^2 + \langle E_2 \rangle^2. \quad (26)$$

In Figure 4 we plot  $\langle \mathbf{E}(x_1, x_2) \rangle^2$  distributions with parameters corresponding to the case  $T = 1.070T_c$  and  $R = 2\text{fm}$ . We observe two "volcanos" with quarks hidden in their bottoms. These two spherically symmetrical in coordinate space distributions are defined as

$$E(r) = B r^2 K_1(r/\lambda), \quad (27)$$

where  $r$  is a distance from quark or antiquark. The field at quark and antiquark positions is zero. Maximal value of field is

$$E^{\text{max}} = E(1.33\lambda) = 0.63B\lambda^2 \quad (28)$$

In Figure 5 the vector field distribution  $\langle \mathbf{E}(x_1, x_2) \rangle$  is shown in the vicinity of the quark.

In the case (b) the transverse part of the field,  $E_2$ , remains the same (25). Let us calculate using (8) the longitudinal part of the field,  $E_1$ :

$$\begin{aligned} \langle E_1(x_1, x_2) \rangle_{Q\bar{Q}}^{(b)} &= \int_0^R dx'_1 \int_{-\infty}^{\infty} dx'_4 \left( D(h^2) + D_1(h^2) + (h_1^2 + h_4^2) \frac{\partial D_1(h^2)}{\partial h^2} \right) = \\ &= \int_{x_1-R}^{x_1} dh_1 \int_{-\infty}^{\infty} dh_4 (-h_2^2) \frac{\partial D_1}{\partial h^2} = \int_{x_1-R}^{x_1} dh_1 \int_0^{\infty} dh_4 \frac{h_2^2}{h\lambda} D_1 = \\ &= \frac{Bx_2^2}{\lambda} \int_{x_1-R}^{x_1} dh_1 K_0(\sqrt{h_1^2 + x_2^2}/\lambda). \end{aligned} \quad (29)$$

In Figure 6 we plot (29) for  $T = 1.070T_c$  and  $R = 2\text{fm}$  to observe the "double quasistring". The quasistring profile,  $E_1(x_2) \equiv \langle E_1(R/2, x_2) \rangle_{Q\bar{Q}}^{(b)}$  at  $R \rightarrow \infty$ , is

$$E_1(x_2) = \pi B x_2^2 \exp(-|x_2|/\lambda). \quad (30)$$

The field in the centre of quasistring is absent. The maximum value of the field is

$$E_1^{\max} = E_1(2\lambda) = 1.7B\lambda^2. \quad (31)$$

In the coordinate space the quasistring resembles coaxial cable with empty core and tube shell. In Figure 7 we plot  $\langle \mathbf{E}(x_1, x_2) \rangle^{(b)}$  distribution around  $Q$  and  $\bar{Q}$ .

To summarize, we have considered the field distributions in the deconfined phase in the framework of FCM for two different forms of correlation function  $D^{\text{E,NP}}(\mathbf{x}^2, x_4^2)$ , which had substantially more constrained form  $D^{\text{E,NP}}(\mathbf{x}^2 + x_4^2)$ . We might use in general any form of  $D^{\text{E,NP}}(\mathbf{x}^2, x_4^2)$  leaving the string tension (5) be zero. Were we use, e.g., the form

$$D^{\text{E,NP}}(\mathbf{x}^2, x_4^2) = -D_1^{\text{E,NP}}(\mathbf{x}^2, x_4^2) - 2\mathbf{x}^2 \frac{\partial D_1^{\text{E,NP}}(\mathbf{x}^2, x_4^2)}{\partial \mathbf{x}^2}, \quad (32)$$

we would get as the expression for the  $\langle E_1 \rangle$  the superposition of (24) and (29).

## 6 Conclusions

Results of our paper based on the analysis of the lattice data on correlation functions at finite  $T_c$  [1] give a full support of the dynamical picture of deconfinement, which was first suggested in [9].

Namely, confining and deconfining phase according to [9] differ first of all in the vacuum fields, i.e. in the value of the condensate and in the field correlators. It was argued in [9] that color magnetic correlators and their contribution to the condensate is kept intact across the temperature phase transition, while the confining electric part abruptly disappears above  $T_c$ . Both features are present in [1] and in the results of the present paper. Indeed, one can see from Table 6, that the magnetic part of condensate is roughly constant around  $T_c$ . The role of magnetic field above  $T_c$  was mentioned repeatedly in the literature, see recent lattice reviews [10], it reveals itself in particular in creating nonzero spatial string tension [9] and so-called screening hadronic masses – (see [11] and refs. therein).

The situation with electric fields is more subtle, as can be seen from our results. In [9] two possible situations have been considered when nonperturbative part of  $D_1^{\text{E}}$  vanishes

or stay nonzero above  $T_c$ . From Figures 4,6 one can clearly see the field distributions in cases of two possible solutions, (a) and (b), one with vanishing  $D^E$  (NP part of it), another with nonvanishing but oscillating  $D^E$  both yielding zero string tension in the deconfinement region.

In the case (a) the electric contribution to condensate is determined by  $D_1^E$  (Table 5). While  $D^E$  vanishes identically, the  $D_1^E$  correlator is different from zero above  $T_c$  and its contribution to the condensate grows sharply with temperature. Hence the role of  $D_1^E$  appears in creating the sharp rise of the "nonideality" ( $\varepsilon - 3p$ ) just above  $T_c$  (cf. Figure 3). One special remark is due to the regime (b), where  $D^{E,NP}$  is nonzero above  $T_c$  but changing sign. This regime creates "quasistring" with empty core and surrounding it ring (tube) shell at two correlation length distance from the quark axis (Figure 6).

This rather peculiar picture cannot be excluded with our present knowledge, and one should pursue in the search for possible physical effects of such "coaxial quasistrings".

Still the regime (a) seems to be more natural from physical point of view, and one should study in more detail the consequences of the strongly increasing  $D_1^E$  in the deconfining region.

The impossibility of resolving our present ambiguity (regimes (a) and (b)) calls for further numerical and analytical studies. It is necessary for understanding of the dynamics of the phase transition, where Polyakov loops and hence colorelectric fields may play very important role.

The authors are grateful to A.Di Giacomo for useful remarks and suggestions, the partial support of grants RFFI 00-02-17836 and 00-15-96786 is gratefully acknowledged.

## References

- [1] A.Di Giacomo, E.Meggiolaro and H.Panagopoulos, preprint IFUP-TH 14/96, hep-lat/9603018.
- [2] H.G.Dosch, V.I.Shevchenko and Yu.A.Simonov, hep-ph/0007223.
- [3] A.Di Giacomo, M.Maggiore and S.Olejnik, Phys.Lett. **B236**, 199 (1990); Nucl.Phys. **B347**, 441 (1990)  
L.Del Debbio, A.Di Giacomo and Yu.A.Simonov, Phys.Lett. **B332**, 111 (1994).
- [4] H.G.Dosch, Phys.Lett. **B190**, 177 (1987);  
H.G.Dosch and Yu.A.Simonov, Phys.Lett. **B205**, 399 (1988);  
Yu.A.Simonov, Nucl.Phys. **B307**, 512 (1988).
- [5] Yu.A.Simonov, Phys.Usp. **39**, 313 (1996).
- [6] Review of Particle Physics, Eur.Phys.J. **C15**, 195 (2000).
- [7] A.Di Giacomo, E.Meggiolaro and H.Panagopoulos, preprint IFUP-TH 12/96, hep-lat/9603017.
- [8] D.S.Kuzmenko and Yu.S.Simonov, Yad.Fiz. **64**, 110 (2001), hep-ph/0010114.
- [9] Yu.A.Simonov, JETP Lett. **54**, 256 (1991);  
Yu.A.Simonov, JETP Lett. **55**, 605 (1992);  
Yu.A.Simonov, Yad.Fiz. **58**, 357 (1995);

Yu.A.Simonov, Lectures at the E.Fermi International School, Varenna 1995, preprint ITEP-37-95.

- [10] F.Karsch, Nucl.Phys.Proc.Suppl. **83**, 14 (2000);  
S.Ejiri, preprint UTCCP-P-95, hep-lat/0011006.
- [11] E.L.Gubankova and Yu.A.Simonov, Phys.Lett. **B360**, 93 (1995).

## List of tables

Table 1: Parameters of  $D^B$ .

T	$0.956T_c$	$0.978T_c$	$1.011T_c$
A, fm <sup>-4</sup>	188.9±2.4	154±2	183.1±3.0
$\lambda_A$ , fm	0.1917±0.0007	0.2047±0.0008	0.1852±0.0008
B, fm <sup>-4</sup>	7.7±0.6	7.7±0.8	1.87±0.13
$\lambda_B$ , fm	0.380±0.008	0.344±0.007	1.11±0.04
a	1.11±0.06	1.46±0.07	0.64±0.03
b	0.34±0.03	0.47±0.04	0.35±0.02
$\chi^2/\text{n}$	0.62	1.28	1.43
T	$1.034T_c$	$1.070T_c$	$1.131T_c$
A, fm <sup>-4</sup>	128.8±2.3	111.9±2.0	150.9±2.5
$\lambda_A$ , fm	0.210±0.001	0.2191±0.0012	0.2009±0.0010
B, fm <sup>-4</sup>	2.92±0.23	3.54±0.29	3.07±0.23
$\lambda_B$ , fm	0.69±0.02	0.631±0.017	0.774±0.024
a	0.92±0.04	1.039±0.043	0.885±0.031
b	0.47±0.03	0.525±0.032	0.506±0.023
$\chi^2/\text{n}$	0.53	1.18	0.58

Table 2: Parameters of  $D^E$  below  $T_c$ .

T	$0.956T_c$	$0.978T_c$
A, fm <sup>-4</sup>	228±4	189.5±4.2
$\lambda_A$ , fm	0.1823±0.0008	0.1812±0.0011
B, fm <sup>-4</sup>	10.8±0.5	14.3±0.6
$\lambda_B$ , fm	0.435±0.011	0.411±0.006
a	3.1±0.4	0.99±0.08
b	0.9±0.2	0.71±0.18
$\chi^2/\text{n}$	0.39	1.7



Table 3: Parameters of  $D^E$  at  $T = 1.011T_c$ .

	(a): $D^{\text{NP}} \equiv 0$	(b): $D_{  }^{\text{NP}} \equiv 0$
B, fm <sup>-4</sup>	2.46±0.24	1.96±0.34
$\lambda_B$ , fm	0.682±0.016	1.072±0.047
a	1.74±0.05	1.36±0.04
b	0.86±0.04	0.68±0.03
$\chi^2/\text{n}$	1.7	1.05

Table 4: Parameters of  $D^E$  above  $T_c$ .

T	1.034 $T_c$	1.070 $T_c$	1.131 $T_c$
B, fm <sup>-4</sup>	80±19	235±53	519±99
$\lambda_B$ , fm	0.121±0.05	0.105±0.004	0.37±0.03
b	0.63±0.03	0.48±0.04	0.41±0.03
$\lambda_b$ , fm	0.86±0.05	1.0±0.1	0.86±0.08
$\chi^2$	0.69	0.9	0.028
(a) a	1.21±0.04	0.94±0.04	0.86±0.03
(a) $\chi^2$	1.26	0.9	2.9
(b) a	0.96±0.04	0.66±0.04	0.61±0.03
(b) $\chi^2$	1.66	0.23	0.56

Table 5: Gluonic condensate.

T	0.956 $T_c$	0.978 $T_c$	1.011 $T_c$	1.034 $T_c$	1.070 $T_c$	1.131 $T_c$
$(A+B)^E$	238.8±4.0	203.8±4.2	2.2±0.3	80±19	235±53	519±99
$(A+B)^B$	196.6±2.5	161.7±2.2	185±3	131.7±2.3	115.4±2.0	154.0±2.5
$\frac{G_2(T)}{G_2}$	1.393±0.015	1.171±0.015	0.60±0.01 <sup>a</sup> 0.59±0.01 <sup>b</sup>	0.69±0.06 <sup>a</sup> 0.422±0.007 <sup>b</sup>	1.12±0.17 <sup>a</sup> 0.370±0.006 <sup>b</sup>	2.16±0.32 <sup>a</sup> 0.493±0.008 <sup>b</sup>

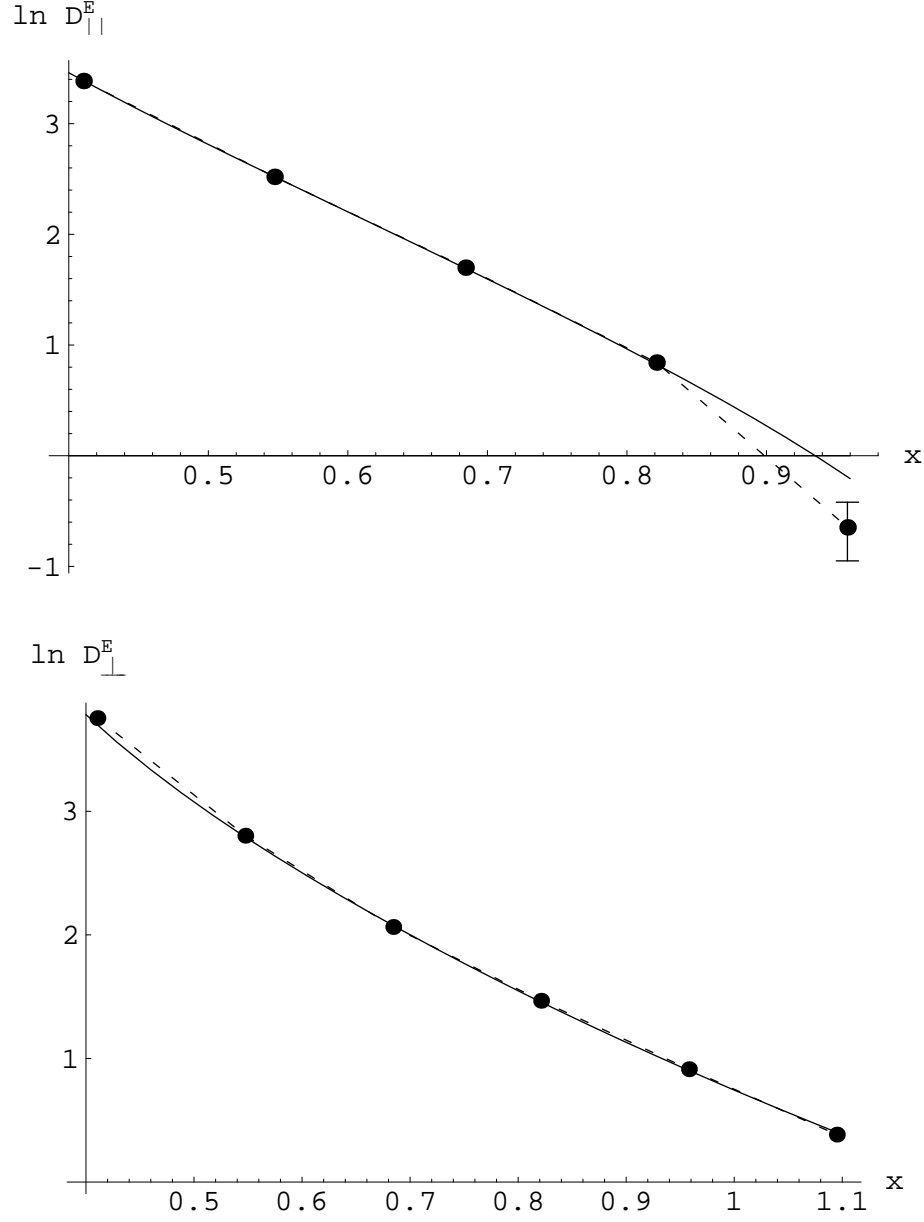


Figure 1: Fitted functions  $\ln D^E_{||}(x)$  and  $\ln D^E_{\perp}(x)$  (shown by solid lines) at  $T = 0.978T_c$ .  $x$  is measured in fm.  $D^E_{||}$  and  $D^E_{\perp}$  are measured in  $\text{fm}^{-4}$ . Data are shown by points joined by dashed lines. Errors of data are comparable with size of the points. The separately shown error is two times enlarged by hand for the improvement of the fit.

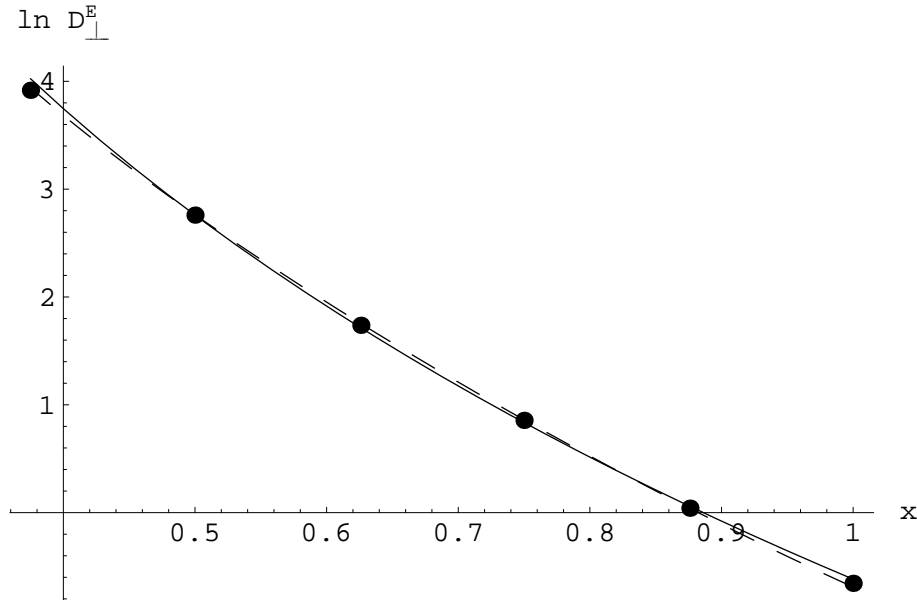


Figure 2: Fitted function  $\ln D_{\perp}^E(x)$ , shown by solid line in case (a) and dashed line in case (b) at  $T = 1.070T_c$ .  $x$  is measured in fm.  $D_{\perp}^E$  is measured in  $\text{fm}^{-4}$ . Data are shown by points joined by dashed lines. Errors of data are comparable with size of the points.

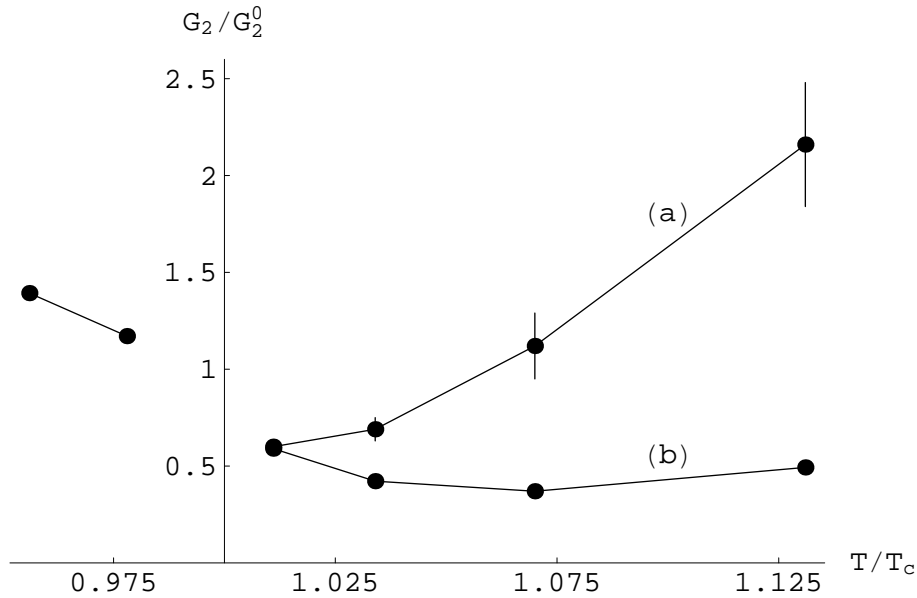


Figure 3: Gluon condensate dependence on  $T/T_c$  near the deconfinement transition. Condensate is measured in its zero temperature value units. In the deconfinement region the magnetic part of condensate does not considerably change. Electric fields give rapidly rising contribution to condensate in case (a) and do not contribute to condensate in case (b).

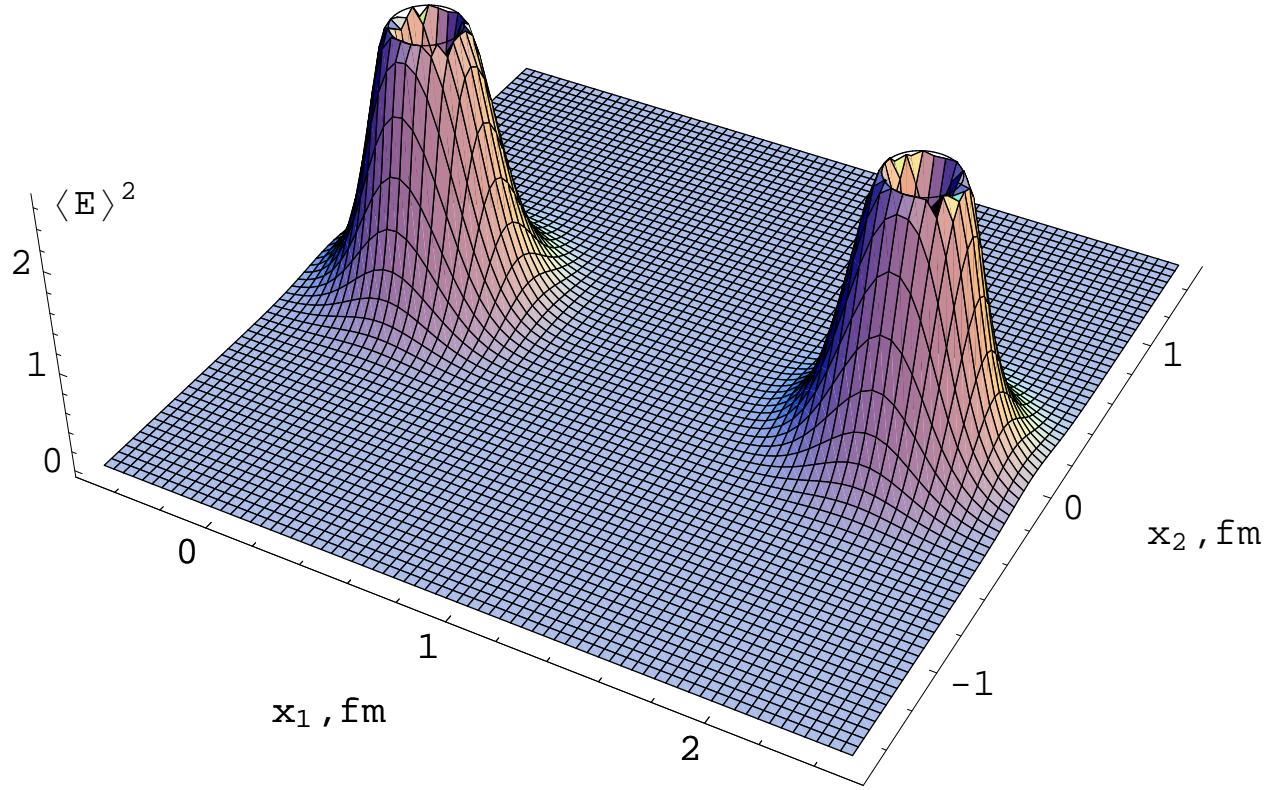


Figure 4: The total field distribution  $\langle \mathbf{E}(x_1, x_2) \rangle^2$ , measured in  $\text{fm}^{-4}$ , in case (a) at  $T = 1.070T_c$ .  $x_1$  and  $x_2$  are measured in fm.  $Q\bar{Q}$  separation  $R = 2\text{fm}$ .

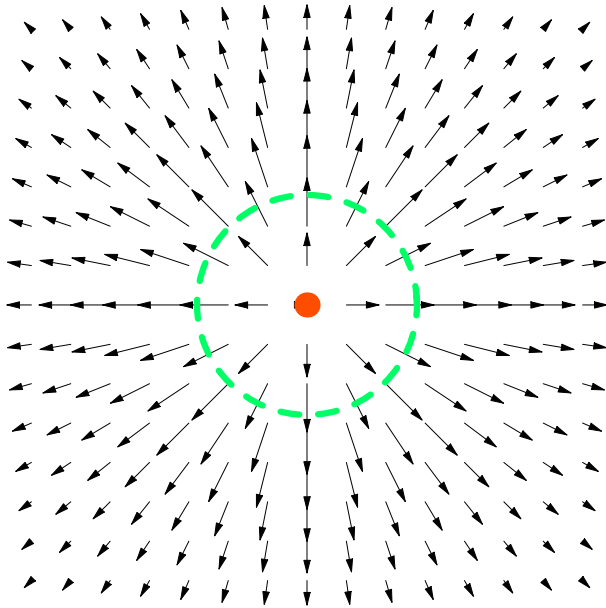


Figure 5: Vector distribution of  $\langle \mathbf{E}(x_1, x_2) \rangle$  in case (a).  $-0.1\text{fm} < x_1 < 2.1\text{fm}$ ,  $-0.5\text{fm} < x_2 < 0.5\text{fm}$ . Quark position is marked with disk. Points of maximal value of field are marked with dashed circle of radius  $1.33\lambda$ .

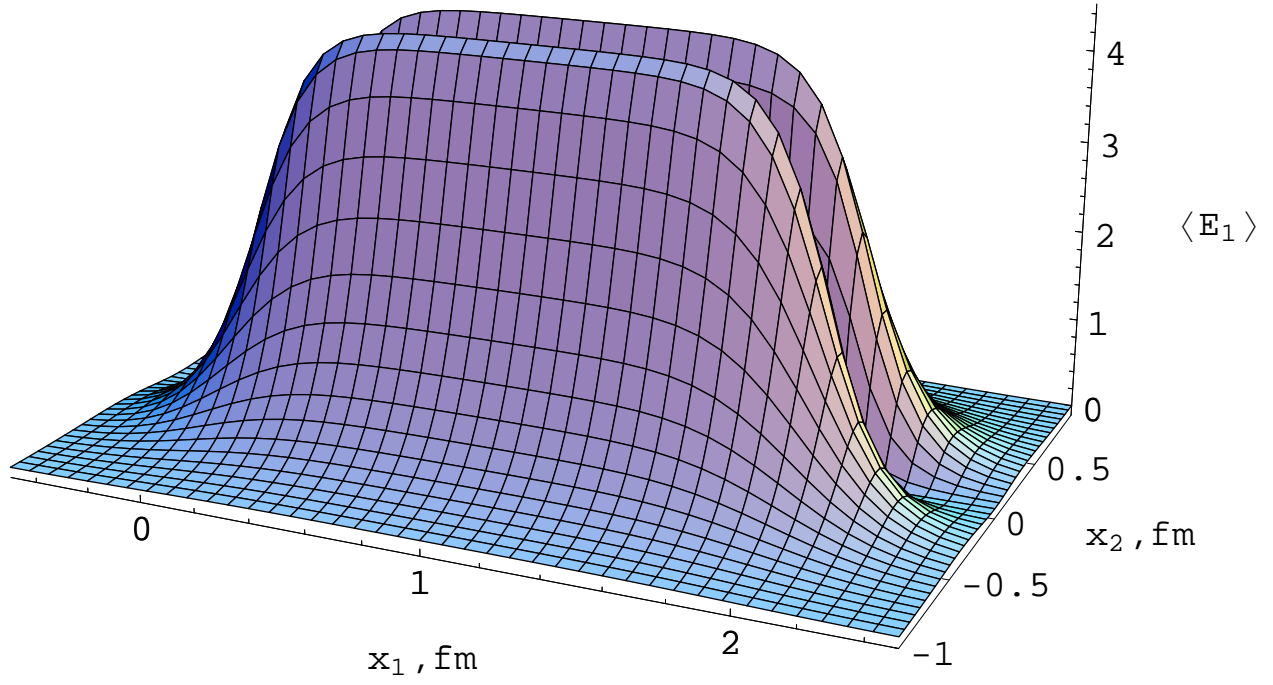


Figure 6: Distribution of  $\langle E_1(x_1, x_2) \rangle$ , measured in  $\text{fm}^{-2}$ , in case (b) at  $T = 1.070T_c$ .

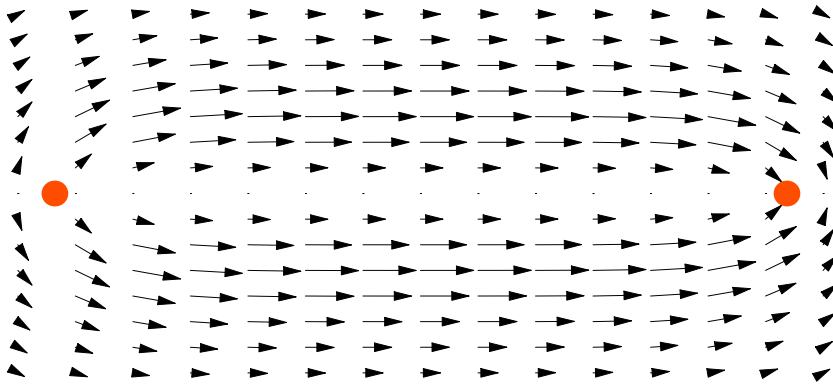


Figure 7: Vector distribution of  $\langle \mathbf{E}(x_1, x_2) \rangle$  in case (b). Positions of  $Q$  and  $\bar{Q}$  are marked with disks.  $-0.1\text{fm} < x_1 < 2.1\text{fm}$ ,  $-0.5\text{fm} < x_2 < 0.5\text{fm}$ .